

Denis Le Bihan, MD, PhD • Jose Delannoy, MD, PhD • Ronald L. Levin, ScD

Temperature Mapping with MR Imaging of Molecular Diffusion: Application to Hyperthermia¹

Efficacy and safety considerations for hyperthermia (HT) cancer therapy require accurate temperature measurements throughout the heated volume. Noninvasive thermometry methods have been proposed, including magnetic resonance (MR) imaging based on the temperature dependence of the relaxation time T1. However, the temperature accuracy achieved to date with T1 measurements does not fulfill the HT requirements (1°C/cm). The authors propose to use molecular diffusion, for which temperature dependence is well known. Molecular diffusion is more sensitive than T1 and can be determined with high accuracy with MR imaging. Diffusion and derived temperature images were obtained with a 2 × 2-mm pixel size in a polyacrylamide gel phantom heated inside the head coil of a clinical 0.5-T whole-body MR imaging system by means of a modified clinical HT device made compatible with the system. Temperatures determined from these images with 0.8-cm² regions of interest were found to be within 0.5°C of those recorded with thermocouples placed inside the gel. The utility of this method in clinical hyperthermia is enhanced by its potential to also help monitor blood perfusion.

Index terms: Hyperthermia • Magnetic resonance (MR), experimental • Magnetic resonance (MR), physics • Therapeutic radiology • Therapeutic radiology, technology

Radiology 1989; 171:853-857

NONINVASIVE and nondestructive temperature imaging in biologic systems may be used in many applications—for instance, in the study and monitoring of tissue interactions in surgical and medical laser procedures (1,2). Another important application is therapeutic hyperthermia (HT). Early biologic and clinical evidence supports the view that, together with chemotherapy or radiation therapy, HT may be helpful in the treatment of some human cancers (3). Although promising results have been obtained, the clinical use of deep-seated HT treatments has been limited, mainly due to a lack of temperature control (4). Indeed, the effectiveness of HT treatment depends on reaching a minimum temperature in the tumor (>42°C), while safety considerations limit the maximum temperature permissible in normal tissues (<42°C). Therefore, temperature should be monitored throughout the heated region. HT requires at least 1-cm spatial resolution and 1°C sensitivity (5). Temperature can be measured accurately (<0.1°C) with thermosensors—such as thermocouples, thermistors, or fiberoptic probes—which can be implanted in heated tissues. These methods are invasive, however, and may be painful and hazardous, so that only a few probes can be used under clinical conditions, limiting the volume that can be investigated. Recently, several noninvasive temperature-monitoring methods were introduced, but none of them satisfactorily fulfills the above-mentioned HT requirements. For example, infrared- or microwave-based measurements allow tempera-

ture to be measured only to a limited depth, while other imaging methods that involve ultrasound or x rays lack sufficient accuracy and resolution (5).

Magnetic resonance (MR) imaging has been proposed for the monitoring of temperature during HT because some physical variables currently accessible to MR imaging are sensitive to temperature (6). Compared with other noninvasive methods, MR imaging has the advantage of producing three-dimensional anatomic images of any part of the body in any orientation with high resolution. It also has the potential to help monitor blood flow at the capillary level (7-9), which is a key factor in the efficacy of clinical HT, since the temperature reached in a tissue depends largely on the ability of the vascular network to transport heat out of the heated region. Furthermore, tissue metabolic changes relative to HT have been shown to be detectable with MR spectroscopy (10). For these reasons, MR imaging seems ideal for the real-time management of clinical HT sessions.

The thermal imaging potential of MR was considered in the past (11-13) with regard to the temperature dependence of MR variables, essentially the spin-lattice relaxation time, or T1, of water (11,12), which has been demonstrated in vitro for different biologic systems (14). Unfortunately, the relationship between T1 and temperature is not simple, mainly due to the multifactorial nature of T1 (2,15). Furthermore, accurate measurements of T1 from MR images are difficult to make because of a high environmental sensitivity, dominated by the effects of radio-frequency field inhomogeneities in the imaged volume (16). The applicability of this

¹ From the Diagnostic Radiology Department, Warren Grant Magnuson Clinical Center (D.L.B.), Radiation Oncology Branch/COP/DCT, National Cancer Institute (J.D.), and the Biomedical Engineering and Instrumentation Branch/DRS (J.D., R.L.L.), Bldg 10, Rm 1C660, National Institutes of Health, Bethesda, MD 20892. From the 1988 RSNA annual meeting. Received November 21, 1988; revision requested January 13, 1989; revision received February 6; accepted February 8. **Address reprint requests to D.L.B.**

© RSNA, 1989

Abbreviations: HT = hyperthermia, MAPA = miniannular phased array, ROI = region of interest, TR = repetition time, TE = echo time.

technique, therefore, seems to be limited because a 1% change in T1 must be measured in order to detect a 1°C change in temperature (5,11,12). The use of chemical shift-resolved MR imaging has also been proposed on the basis of experiments, but this method has even more severe limitations in vivo (17).

We instead propose to use molecular diffusion of water as a thermal indicator in measuring and imaging temperature. There is a direct relationship between temperature and the diffusion coefficients that quantify thermal Brownian motion. Molecular diffusion can be measured with MR to high accuracy (18), and, recently, MR imaging techniques were developed to quantitatively image diffusion in vivo (19-21). The purpose of this study was to demonstrate the feasibility of temperature monitoring with MR imaging of molecular diffusion and to show that the HT requirements for temperature monitoring may be fulfilled. The theory was supported by the results of phantom experiments. A modified clinical HT device working in combination with a whole-body clinical MR imaging unit was used to test the method.

PRINCIPLE

Relation between Temperature and Diffusion

On the basis of the Stokes-Einstein relation between viscosity and the translational self-diffusion coefficient D , the following temperature dependence of D can be used (22,23):

$$D \propto \exp(-E_a/kT), \quad (1)$$

where k is the Boltzmann constant, E_a is the activation energy for translational molecular diffusion, and T is temperature. Temperature changes thus induce viscosity and diffusion coefficient changes, which can be calculated by differentiation of Equation (1), assuming small variations of E_a with T :

$$dD/D = (E_a/kT)dT/T. \quad (2)$$

From Equation (2) it is obvious that temperature changes may be detected from diffusion coefficient measurements.

MR Imaging of Molecular Diffusion

Diffusion coefficients can be measured and imaged with MR (19-21). The effect of molecular diffusion in

the presence of a magnetic field gradient on MR spin-echo signals was described long ago (24,25). Diffusion induces an amplitude attenuation of the MR signal caused by a loss of phase coherence among precessing spins that move randomly along the direction of the gradient. This amplitude attenuation A depends only on the diffusion coefficient D and the gradient, so that

$$A = \exp(-b \cdot D), \quad (3)$$

where b is a factor that can be calculated from gradient characteristics (strength and duration) (18-20,24,25). Stejskal and Tanner (18) introduced a diffusion measurement method that used pulsed magnetic field gradients, thereby improving the sensitivity of measurements and allowing smaller values of diffusion coefficients to be determined. More recently, these concepts were extended to MR imaging (19,20) and applied to a water molecule diffusion mapping method based on two MR images differently sensitized to diffusion by the presence of specially designed gradient pulses (Fig 1). Under these conditions, the diffusion image $D_{x,y}$ is derived from the relation

$$D_{x,y} = \log(A_{1x,y}/A_{0x,y})/(b_0 - b_1), \quad (4)$$

where b_0 and b_1 are the calculated gradient factors of both images and A_1/A_0 is the amplitude attenuation ratio in each pixel. The ratio A_1/A_0 is equal to the signal amplitude ratio S_1/S_0 of both images because both images are identical with respect to all other MR imaging variables, namely, the repetition time (TR) and the echo time (TE) of the spin-echo imaging sequence used. Other MR imaging sequences, such as steady-state free precession (SSFP), which allows very short acquisition times, may also be used (26-28).

Temperature Imaging

A map of temperature changes ($T - T_0$)_{x,y} can thus be obtained from two diffusion images $D_{x,y}$ and $D_{0x,y}$, one obtained at the reference temperature $T_0(D_{0x,y})$, and one obtained at a different temperature $T(D_{x,y})$, such that

$$(T - T_0)_{x,y} = (kT_0^2/E_a) \cdot [(D - D_0)/D_0]_{x,y}, \quad (5)$$

where one assumes small temperature variations ($T - T_0 \ll T_0$) and that E_a is approximately constant.

In an HT experiment, T_0 would be

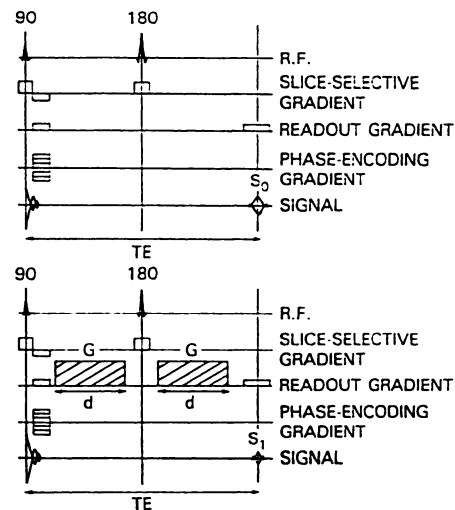


Figure 1. Diffusion imaging sequence. Diffusion images can be calculated from the signal ratio S_1/S_0 of two images obtained from two spin-echo imaging sequences differently sensitized to diffusion by the presence of additional magnetic field gradient pulses. G = intensity, d = duration, R.F. = radio frequency.

the local tissue temperature before heating, while T would be the local tissue temperature during heating. Substitution of published values of E_a (0.2 eV at 20°C) (22,23) in Equation (5) shows that sensitivity of temperature mapping from diffusion measurements is high, since a 1°C change in temperature corresponds to a 2.4% change in the diffusion coefficient.

MATERIALS AND METHODS

Experiments were conducted first to validate Equation (5), on which the method is based, and to check the sensitivity of this MR imaging diffusion technique for temperature measurement. A phantom was designed with MR imaging variables close to those of biologic tissues with respect to water content, relaxation times, and diffusion coefficient. It consisted of a polyacrylamide gel (7.5% polyacrylamide) with 5 mmol/L of copper (II) sulfate (28) contained in a cubic Plexiglas box (10 × 10 × 10 cm). The phantom was placed within the central homogeneous radio-frequency field of a 30-cm-diameter imaging coil that served as both the transmitter and receiver. A temperature gradient (about 1°C/cm) was induced between the two opposite faces of the phantom in the direction of the main magnetic field by water streams at two different temperatures circulating in compartments placed at the opposite faces. The phantom and the water compartments were encased in a block of polystyrene to afford thermal insulation. Temperatures were monitored with copper-constantan thermocouples placed within catheters located along the direction of the induced

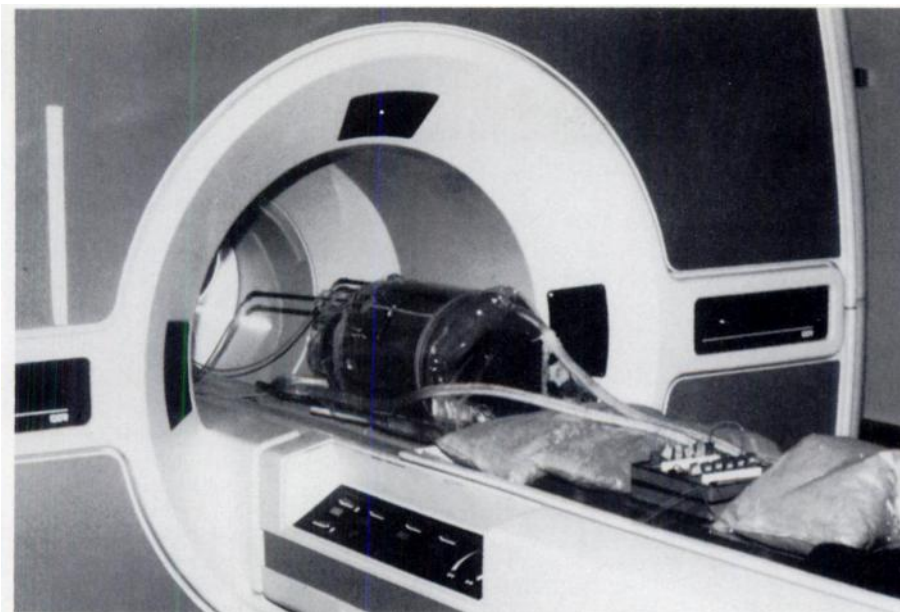


Figure 2. Experimental HT device working together with the MR imaging unit. The temperature imaging method was tested in real conditions with a modified HT radio-frequency applicator (MAPA) designed for human limb tumor treatment. This device, which uses electromagnetic waves for heating, was made entirely compatible with the MR imaging unit, mechanically and electrically, and can be attached to the patient mobile support. It can be then centered inside the head coil. A gel phantom was used, and heating and imaging were performed approximately simultaneously in a time-sharing manner.

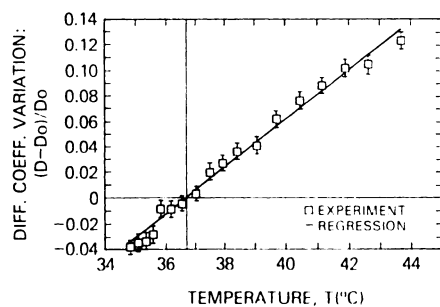


Figure 3. Experimental validation of the relation between diffusion and temperature. The relative change in the diffusion coefficient $(D - D_0)/D_0$ measured at different locations inside a gel phantom in which a thermal gradient ($1^\circ\text{C}/\text{cm}$) was induced is plotted against the temperature measured from miniature thermocouples placed at the same locations. The accuracy of the temperature from the thermocouples was 0.1°C , while the accuracy of the calculated diffusion coefficients with 0.8-cm^2 ROIs was 1%. The relation was linear, as expected from Equation (5). The reference temperature T_0 was 36.7°C ($D_0 = 2.22 \times 10^{-3} \text{ mm}^2/\text{sec}$), and the activation energy E_a calculated from the slope of the plot was 0.154 eV .

thermal gradient. The temperatures T_0 and T were measured, respectively, before and during heating every 5 mm along the thermal gradient.

Diffusion images were obtained in the catheter plane before and during the presence of the thermal gradient. The relative changes in the diffusion coefficient D were averaged from these diffusion images every 5 mm in the direction of the thermal gradient, with 0.8-cm^2 regions of

interest (ROIs). Two series of experiments were performed: One centered around room temperature ($T_0 = 23.8^\circ\text{C}$), and the other centered around normal body temperature ($T_0 = 36.7^\circ\text{C}$), to which the gel was first uniformly heated.

Temperature images were then obtained under more realistic HT conditions with a clinical HT device. MR coils cannot be used directly for HT studies because they are especially inefficient for generating tissue heating when properly designed for MR imaging applications. Therefore, the idea of this study was to use an HT device distinct from the MR coil. Manipulation of an HT device within the magnet bore is not trivial but is a surmountable challenge (29). We used a cylindrical phantom (12 cm in diameter and 60 cm long) made of the same gel, but heating was induced by means of an HT applicator (miniannular phased array [MAPA]) with high-frequency electric fields (Fig 2). The MAPA was originally designed for the treatment of limb tumors (30) and consists of a cylindrical array of eight dipole elements that are normally activated in phase and with equal amplitude in the frequency range of 100–200 MHz. Under these conditions, the electric fields of the dipoles constructively interfere and maximize the specific absorption rate along the central axis of the applicator (30). We made an MAPA applicator compatible with the MR imaging unit by removing all of its ferromagnetic parts and rewiring it electrically. The modified MAPA was fixed to the mobile patient support table of the MR imaging unit, so that it could be centered inside the MR head coil. Cross talk between the two radio-frequency units (HT at 168

MHz and MR imaging at 21 MHz) was minimized with the aid of several radio-frequency filters (29).

Electric coupling between the HT applicator and the phantom was obtained by filling the space between them with a "bolus" that contained water cooled with a heat exchanger and a closed-loop circulation system. Manganese chloride (1 mmol/L) was added to the bolus water to minimize the signal coming from it and thereby the possibility of motion artifacts. Heating was induced in the phantom, previously stabilized at room temperature, by long radio-frequency HT pulses (about 700 msec) with a power level of 120–300 W and interleaved with the image acquisition process in a time-sharing manner by means of a switch box and the built-in gating capability of the MR imaging unit. Under these conditions a temperature elevation of about 15°C was obtained in the phantom after 30 minutes of heating. Miniature thermocouples (Sensortek; Bailey, Clifton, NJ) placed within 11 catheters spaced 1 cm apart in a plane parallel to the major axis of the phantom were used to validate the MR imaging temperature measurements.

In both experiments, temperature was stabilized ($<0.3^\circ\text{C}$ change) during the MR imaging acquisition process. Diffusion and resulting temperature images were obtained on a clinical 0.5-T whole-body MR imaging system (Magniscan 5000; Thomson-CGR, Paris) at 21 MHz. Diffusion images were obtained as previously described (19,20) from two different diffusion sensitized spin-echo images ($\text{TR} = 800 \text{ msec}$, $\text{TE} = 140 \text{ msec}$, 128×128 acquisition matrix, 1-cm section thickness), allowing images to be obtained with a $2 \times 2\text{-mm}$ spatial resolution. The acquisition time for each image was 3 minutes, 25 seconds. These diffusion and temperature images were calculated immediately after each acquisition according to Equations (4) and (5), respectively, with a VAX-11/730 computer (Digital Equipment, Maynard, Mass) coupled to an MSP-3000 array processor (Computer Design and Applications, Waltham, Mass).

RESULTS

The plot of the relative change $([D - D_0]/D_0)$ in the diffusion coefficient versus the absolute temperature change $(T - T_0)$, as obtained in the first experiments, is shown in Figure 3. As expected, the relation was found to be linear. The activation energy E_a of water in the gel was obtained from the slope of the plot by means of Equation (5). The values were $0.212 \text{ eV} \pm 0.004$ at $T_0 = 23.8^\circ\text{C}$ and $0.154 \text{ eV} \pm 0.004$ at $T_0 = 36.7^\circ\text{C}$, which agree well with published data (0.21 eV at 20°C) associated with the diffusion coefficient of water (22,23). D_0 was $(1.76 \pm 0.02) \times 10^{-3} \text{ mm}^2/\text{sec}$ and $(2.22 \pm 0.02) \times 10^{-3} \text{ mm}^2/\text{sec}$ at 23.8°C and 36.7°C , re-

spectively. The measurement error in determination of the relative change in D with 0.8-cm^2 ROIs was 1%, which corresponds to a 0.5°C uncertainty in temperature.

A transverse-section temperature image obtained in the second experiment is shown in Figure 4. Temperatures can be accessed instantaneously on a pixel-by-pixel basis with a mobile cursor or with ROIs. The signal-to-noise ratio can be improved by increasing pixel size; high spatial resolution in HT temperature imaging is not really necessary when high-resolution anatomic images and temperature images are obtained together. The profile obtained from the average of two ROIs, 10 mm wide, recorded on both sides of each catheter plane, was compared with the actual profile measured with the thermocouple probes (Fig 5). Each measurement corresponded again to a 0.8-cm^2 ROI, and this correlation was also found to be excellent.

DISCUSSION

These experiments demonstrate the ability to measure temperature changes by means of molecular diffusion imaging with MR. Temperature mapping can be achieved in three dimensions in the multisection mode and fulfills the HT requirements ($1^\circ\text{C}/\text{cm}$).

The sensitivity of temperature determination by means of diffusion appears to be greater than that of procedures based on T1 (11,12,15). This increased sensitivity may be due to the different relationships between diffusion and temperature and T1 and temperature, since the activation energy of diffusion and relaxation are different. T1 relaxation time depends in part on diffusion. However, in biologic tissues, the diffusion factor that might predominate in T1 relaxation is rotational diffusion (11,14,15), which is less sensitive to temperature than translational diffusion (15,22,23). Furthermore, there are many other contributions to T1, so that its temperature dependence may not be easy to derive. There is, for instance, an MR imaging frequency dependence in the relationship of T1 with temperature (15,31) that does not apply to translational diffusion. In addition, T1 determinations with MR imaging are often inaccurate. Errors in T1 measurements are related to difficulties in obtaining homogeneous MR radio-frequency fields throughout the imaged section (16). These difficulties disappear in the

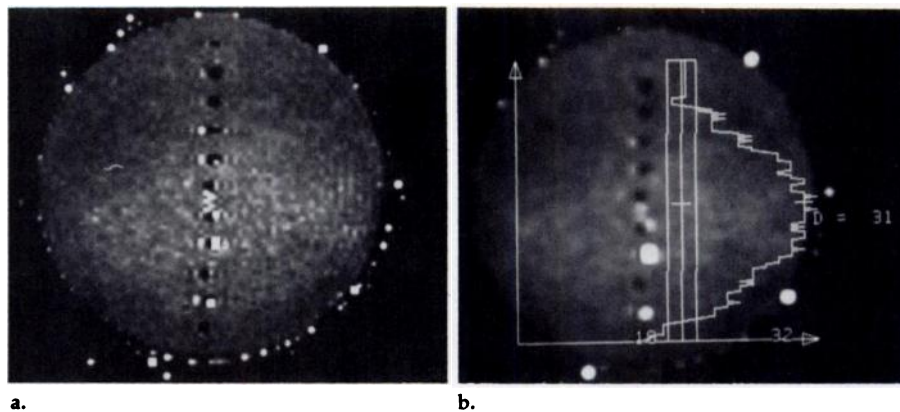


Figure 4. MR temperature images. The temperature image (a) was obtained from a gel phantom heated with the HT device shown in Figure 2. The acquisition time was $2 \times 3\frac{1}{2}$ minutes, and the spatial resolution was 2×2 mm. Maximum power deposition was induced at the center of the phantom, as expected from the type of applicator used. The dark spots in the middle of the image correspond to the position of the catheters used to place thermocouples. Temperature can be measured on the basis of pixels or ROIs. Some features of the image display system (smoothing, temperature profile along a given direction) may improve the presentation of the data (b).

diffusion imaging method because it uses two MR imaging sequences that are identical as far as the radio-frequency field is concerned (19,20). Under these conditions the signal imperfections cancel one another. Diffusion measurements may therefore be more accurate than T1 determinations from MR images, despite less favorable signal-to-noise ratios.

The acquisition time needed in these experiments ($2 \times 3\frac{1}{2}$ minutes) may appear long for true real-time temperature mapping. Moreover, more accurate temperature determination requires higher signal-to-noise ratios obtained by the averaging of multiple acquisitions or by the determination of diffusion coefficients from multiple measurements. Much shorter acquisition times (about 1 minute) could, however, be achieved with recently developed fast diffusion-imaging techniques (26,27). Another benefit of fast imaging methods would be to decrease the sensitivity of diffusion imaging to motion artifacts. This high sensitivity to motion artifacts is related to the presence of the strong and long gradient pulses used to emphasize diffusion effects. Because of these gradient pulses, important dephasings may be generated by the moving parts of the imaged object. Artifacts are produced when these dephasings are temporally incoherent (ie, different from one another between successive acquisition cycles), even when motion is spatially coherent. Therefore, diffusion images have so far been successfully obtained only in parts of the body that are approximately motion free, such as in extremities, or when temporal inco-

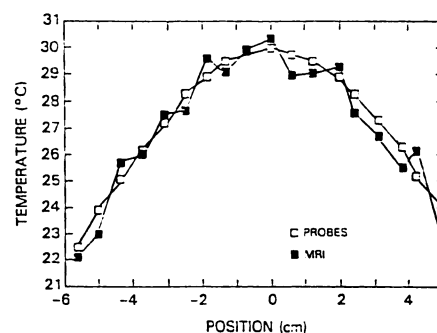


Figure 5. Correlation between MR imaging and invasive temperature measurements. The mean temperature profile on the MR temperature image shown in Figure 4 was obtained by means of two ROIs, 10 mm wide, recorded on both sides of each catheter line, and was plotted together with the temperature profile obtained with the probes placed inside the catheters.

herences can reasonably be eliminated (ie, when motion is sufficiently periodic to allow acquisition cycles to be gated, such as cardiac gating in the brain) (8). Similar artifacts may also result from gradient instabilities. In practice, variations among the diffusion measurements must be less than 5% in order to detect 1°C temperature changes. Gradient coils shielded from eddy current effects are obviously preferable, although the gradient coils used in this preliminary study were the regular gradient coils of the MR unit.

To apply this method in vivo for clinical HT, the relationship between T and D (Equation [5]) needs to be validated in biologic tissues. This relation has been established for free water molecules. Measured diffusion coefficients can be affected in vivo by restricted diffusion phenomena relat-

ed to compartmental effects in water mobility (32). The non-Brownian character of restricted diffusion may affect its relation with temperature. However, restricted diffusion effects may be limited, if necessary, by shortening TE in diffusion measurements (20,21). Furthermore, the use of Equation (5) for temperature measurement assumes that E_a has been previously determined in biologic tissues and that E_a is constant in the temperature range used for clinical HT. If the activation energy were dependent on the material type and temperature, it would be necessary to have a map of E_a and the initial absolute temperature (T_0) to calculate the final temperature image $T_{x,y}$. Fortunately, previous studies (23) have shown that over a temperature range of 5°–40°C, the E_a of intracellular water was about 0.21 eV, which is practically the same as that of pure liquid water (22,23) and equal to the amount of energy required to break two hydrogen bonds. The nonnegligible change in E_a we observed in our gel phantom between 23.8° and 36.7°C was probably due to a temperature-induced change in physical structure. Finally, only a map of the temperature change is obtained with this method. If one wants to determine the absolute temperature after heating, the initial absolute temperature must be known. A reasonable solution in the case of clinical HT would be to bring the region to be treated to a known uniform temperature by surrounding it with a water bolus at the body temperature.

Furthermore, diffusion coefficients should be measured especially carefully in vivo. Measurements may be affected by other intravoxel incoherent motions of water present in biologic tissues (8,20). In particular, separation of the contribution of diffusion from that of blood microcirculation must be achieved with an appropriate algorithm. Microcirculation-free diffusion measurements can be obtained by means of additional gradient pulses in both sequences (S_0 and S_1) so that the signal contribution of the circulating blood flow component is fully eliminated (20). On the other hand, perfusion imaging may be useful in HT studies, since blood circulation plays an important role in the thermal clearance

of normal and pathologic tissues (33). It has been shown that, by means of the same method, diffusion and perfusion can be separately and simultaneously imaged (20). Separation between diffusion and perfusion requires at least one extra sequence and is therefore time consuming. It may thus be difficult to apply in its current form to clinical HT, in which time is a critical factor; however, faster methods for imaging intravoxel incoherent motions have the potential for simultaneously helping monitor temperature by diffusion and tissue perfusion, which are the two key variables of clinical HT.

Obviously, the applications of the method are not limited to HT. Among potential applications is detection of possible temperature changes or hot spots induced by the radio-frequency pulses used in MR imaging (34). Laser-tissue interaction studies (1,2) in which power deposition and heating are key features may also benefit from this temperature imaging method. ■

References

1. Svaasand LO, Boerslid T, Oeveraasen M. Thermal and optical properties of living tissue: application to laser-induced hyperthermia. *Laser Surg Med* 1985; 5:589–602.
2. Jolesz FA, Bleier AR, Jakab P, Ruenzel PW, Huttli K, Jako GJ. MR imaging of laser-tissue interactions. *Radiology* 1988; 168:249–253.
3. Hahn GM. Thermal enhancement of the actions of anticancer agents. In: Becker FF, ed. *Hyperthermia and cancer*. 2d ed. New York: Plenum, 1982; 55–86.
4. Cetas TC. Will thermometric tomography become practical for hyperthermia treatment monitoring? *Cancer Res* 1984; 44:4805–4808.
5. Gibbs FA, Sapozink MD, Stewart JR. Clinical thermal dosimetry: why and how. In: Overgaard J, ed. *Hyperthermic oncology*. Vol 2. Philadelphia: Taylor and Francis, 1984; 155–167.
6. Knuttel B, Juretschke HP. Temperature measurements by nuclear magnetic resonance and its possible use as a means of in vivo non-invasive temperature measurement and for hyperthermia treatment assessment. *Recent Results Cancer Res* 1986; 101:109–118.
7. Ahn CB, Lee SY, Nalcioglu O, Cho ZH. The effects of random directional distributed flow in NMR imaging. *Med Phys* 1987; 14:43–48.
8. Le Bihan D, Breton E, Lallemand D, Aubin ML, Vignaud J, Laval-Jeantet M. Separation of diffusion and perfusion in intravoxel incoherent motion MR imaging. *Radiology* 1988; 168:497–505.
9. Young IR, Hall AS, Bryant DJ, et al. Assessment of brain perfusion with MR imaging. *J Comput Assist Tomogr* 1988; 12:721–727.
10. Vaupel PW, Okunieff PG, Neuringer LJ. Hyperthermia-induced changes in tumor pH and energy status level evaluated by in vivo ³¹P-nuclear magnetic resonance spectroscopy (abstr). In: *Book of abstracts: Society of Magnetic Resonance in Medicine 1988*. Vol 1. Berkeley, Calif: Society of Magnetic Resonance in Medicine, 1988; 412.
11. Parker DL, Smith V, Sheldon P, Crooks LE, Fussell L. Temperature distribution measurements in two-dimensional NMR imaging. *Med Phys* 1983; 10:321–325.
12. Dickinson RJ, Hall AS, Hind AJ, Young IR. Measurement of changes in tissue temperature using MR imaging. *J Comput Assist Tomogr* 1986; 10:468–472.
13. Tanaka H, Eno K, Kato H, Ishida T. Possible application of non-invasive thermometry for hyperthermia using NMR. *Nippon Acta Radiol* 1981; 41:897–899.
14. Lewa CJ, Majeska Z. Temperature relationships of proton spin-lattice relaxation time T₁ in biological tissues. *Bull Cancer (Paris)* 1980; 67:525–530.
15. Bottomley PA, Forster TH, Argersinger RE, Pfeifer LM. A review of normal tissue hydrogen NMR relaxation times and relaxation mechanisms from 1–100 MHz: dependency on tissue type, NMR frequency, temperature, species, excision, and age. *Med Phys* 1984; 11:425–448.
16. Young IR, Bryant DJ, Payne JA. Variations in slice shape and absorption as artifacts in the determination of tissue parameters in NMR imaging. *Magn Reson Med* 1985; 2:355–389.
17. Hall LD, Talagala SL. Mapping of pH and temperature distribution using chemical-shift-resolved tomography. *J Magn Reson* 1985; 65:501–505.
18. Stejskal EO, Tanner JE. Spin diffusion measurements: spin echoes in the presence of a time-dependent field gradient. *J Chem Phys* 1965; 42:288–292.
19. Le Bihan D, Breton E. Imagerie de diffusion in-vivo par resonance magnetique. *CR Acad Sci (II) (Paris)* 1985; 301:1109–1112.
20. Le Bihan D, Breton E, Lallemand D, Grenier P, Cabanis E, Laval-Jeantet M. MR imaging of intravoxel incoherent motions: application to diffusion and perfusion in neurological disorders. *Radiology* 1986; 161:401–407.
21. Taylor DG, Bushnell MC. The spatial mapping of translational diffusion coefficients by the NMR imaging technique. *Phys Med Biol* 1985; 30:345–349.
22. Simpson JH, Carr HY. Diffusion and nuclear spin relaxation in water. *Phys Rev* 1958; 111:1201–1202.
23. Chang DC, Rorschach HE, Nichols BL, Hazlewood CF. Implications of diffusion coefficient measurements for the structure of cellular water. *Ann NY Acad Sci* 1973; 204:434–443.
24. Hahn EL. Spin-echoes. *Phys Rev* 1950; 80:580–594.
25. Carr HY, Purcell EM. Effects of diffusion on free precession in nuclear magnetic resonance experiments. *Phys Rev* 1954; 94:630–638.
26. Le Bihan D. Intravoxel incoherent motion imaging using steady-state free precession. *Magn Reson Med* 1988; 7:346–351.
27. Le Bihan D, Turner R, MacFall J. Effects of intravoxel incoherent motions (IVIM) in steady-state free precession (SSFP) imaging: application to molecular diffusion imaging. *Magn Reson Med* (in press).
28. De Luca F, Maraviglia B, Mercurio A. Biological tissue simulation and standard testing material for MRI. *Magn Reson Med* 1987; 4:189–192.
29. Le Bihan D, Delannoy J, Levin RL, Hoult DI. Design, development, and preliminary tests of a hyperthermia device monitored with MR imaging (abstr). In: *Book of abstracts: Society of Magnetic Resonance in Medicine 1988*. Vol 2. Berkeley, Calif: Society of Magnetic Resonance in Medicine, 1988; 858.
30. Turner PF. Mini-annular phased array for limb hyperthermia. *IEEE Trans MTT* 1986; 34:508–513.
31. Fung BM. Proton and deuteron relaxation of muscle water over wide ranges of resonance frequencies. *Biophys J* 1977; 18:235–239.
32. Stejskal EO. Use of spin-echoes in a pulsed magnetic field gradient to study anisotropic, restricted diffusion and flow. *J Chem Phys* 1965; 43:3597–3603.
33. Hahn GM. Blood flow. In: Field SB, Franconi C, eds. *Physics and technology of hyperthermia*. Boston: Martinus Nijhoff, 1987; 441–447.
34. Shellock FG, Cruess JV. Temperature, heart rate, and blood pressure changes associated with clinical MR imaging at 1.5 T. *Radiology* 1987; 163:259–262.